Applied Clay Science 211 (2021) 106189

Contents lists available at ScienceDirect

Applied Clay Science

journal homepage: www.elsevier.com/locate/clay

Research Paper

Selenium isotope fractionation during adsorption onto montmorillonite and kaolinite

Wenpo Xu [a], Hai-Bo Qin [a,c,*], Jian-Ming Zhu [b,**], Thomas M. Johnson [d], Decan Tan [a], Chengshuai Liu [a], Yoshio Takahashi [c,e]

[a] State Key Laboratory of Environmental Geochemistry, Institute of Geochemistry, Chinese Academy of Sciences, Guiyang 550081, China
[b] State Key Laboratory of Geological Processes and Mineral Resources, China University of Geosciences, Beijing 100083, China
[c] Department of Earth and Planetary Science, Graduate School of Science, The University of Tokyo, Hongo, Bunkyo-ku, Tokyo 113-0033, Japan
[d] Department of Geology, University of Illinois at Urbana-Champaign, Urbana, IL 61801, USA
[e] Photon Factory, Institute of Materials Structure Science, High Energy Accelerator Research Organization (KEK), Tsukuba, Ibaraki 305-0801, Japan

ARTICLE INFO

Keywords:
Adsorption
Montmorillonite
Kaolinite
Se isotope fractionation
Extended X-ray absorption fine structure (EXAFS)

ABSTRACT

Adsorption is an important geochemical process constraining the global cycling of selenium (Se) in the environment. However, Se isotope fractionation during adsorption onto clay minerals has been rarely reported. In this study, Se isotope fractionation during adsorption onto montmorillonite and kaolinite was investigated by a combination of adsorption experiments and extended X-ray absorption fine structure (EXAFS) spectroscopy. Results showed that a small adsorption and negligible isotope fractionation were observed during Se(VI) adsorption on montmorillonite and kaolinite at pH 4.5. By contrast, Se isotope fractionations ($\Delta^{82/76}Se_{dissolved\text{-}adsorbed}$) during the adsorption of Se(IV) on montmorillonite and kaolinite were $\leq 0.23‰$, suggesting that lighter Se(IV) isotopes are preferentially adsorbed onto clay minerals. In addition, different effect of ionic strength on Se (IV) isotope fractionation was found between kaolinite and montmorillonite, which is likely ascribed to distinct surface charge and structure between the two clay minerals. These little or no Se isotope fractionations could be related to the fact that Se oxyanions are mainly adsorbed on montmorillonite and kaolinite via the outer-sphere complexation, as revealed by Se K-edge EXAFS analysis. The findings from this study would help further identify and constrain the key geochemical processes causing Se isotope variations, providing a foundation to develop Se isotope as a proxy for biogeochemical cycling of Se in the natural environment.

1. Introduction

Selenium (Se) is a trace element with considerable concerns, since it is an essential micronutrient for organisms at low concentrations, but it becomes toxic at slightly higher concentrations (e.g., Zhu et al., 2008b; Fordyce, 2013; Qin et al., 2013). Se can be found in -II, 0, IV, and VI valences in natural settings (Elrashidi et al., 1987; Zhu et al., 2004, 2012; Qin et al., 2012a,2017a,2017b). In soils and water, the thermodynamically favorable selenite [Se(IV)] and selenate [Se(VI)] oxyanions can be present (e.g., Séby et al., 2001; Fordyce, 2013). The fate of dissolved Se(IV) and Se(VI) oxyanions in supergene systems is primarily controlled by the interaction with mineral phases, such as adsorption and incorporation process (Balistrieri and Chao, 1990; Francisco et al., 2018).

Selenium has six stable isotopes: ^{74}Se, ^{76}Se, ^{77}Se, ^{78}Se, ^{80}Se and ^{82}Se, whose abundances are 0.889%, 9.366%, 7.635%, 23.772%, 49.607% and 8.731%, respectively. During the past two decades, multiple-collector inductively coupled plasma mass spectrometry (MC-ICP-MS) and analytical techniques (especially Se double spikes technique) have been largely improved, which allows high-precision measurements of Se isotopes in environmental and geological samples. Thus, stable isotope geochemistry of Se represents a new tool to trace the fate of Se. Previous studies have reported Se isotope compositions ($\delta^{82/76}Se = (^{82}/^{76}Se_{sample}/^{82/76}Se_{standard} - 1) \times 1000$) in various reservoirs, such as meteorites, magmatic rocks, sedimentary rocks, soils, oceanic sediments, seawater, ocean ferromanganese nodules and surface water, with a lager variation from −14.20‰ to +11.37‰ (e.g., Johnson et al., 2000; Rouxel et al., 2002; Clark and Johnson, 2010; Schilling et al., 2011; Zhu et al., 2014;

* Corresponding author at: State Key Laboratory of Environmental Geochemistry, Institute of Geochemistry, Chinese Academy of Sciences, Guiyang 550081, China.
** Corresponding author.
E-mail addresses: qinhaibo@vip.gyig.ac.cn (H.-B. Qin), jmzhu@cugb.edu.cn (J.-M. Zhu).

https://doi.org/10.1016/j.clay.2021.106189
Received 19 January 2021; Received in revised form 29 April 2021; Accepted 7 June 2021
Available online 24 June 2021

Chang et al., 2017). Furthermore, Se isotopes fractionations derived by different biogeochemical processes have been investigated. Microbial or abiotic reduction of Se oxyanions could yield significant isotope fractionations (1.7–19‰), while other processes such as precipitation, volatilization, oxidation, and adsorption may result in relatively small (< 1.5‰) or no Se isotope fractionations (Johnson et al., 1999; Herbel et al., 2000; Johnson and Bullen, 2003; Schilling et al., 2013; Mitchell et al., 2013; Tan et al., 2020). Se isotopes are gradually becoming a potential proxy for tracing biogeochemical processes and pollution sources of Se, as well as the redox conditions of paleo-oceanography (e.g., Johnson et al., 1999; Mitchell et al., 2012; Zhu et al., 2014; Pogge von Strandmann et al., 2015; Stüeken et al., 2015; Kipp et al., 2017).

Selenium adsorption by many materials, including metal oxides (Fe, Mn, and Al), clay minerals and organic matters, etc., plays an important role in the global cycling of Se in the natural environment (e.g., Bar-Yosef and Meek, 1987; Balistrieri and Chao, 1990; Qin et al., 2012a,2017a). However, to date, limited knowledge is available for Se isotope fractionations caused by adsorption. Only several studies have investigated Se isotope fractionation behavior during the adsorption on Fe, Mn, and Al oxides, and sulfides (Johnson et al., 1999; Mitchell et al., 2013; Xu et al., 2020).

Clay minerals (e.g., montmorillonite and kaolinite) are widely distributed in terrestrial environments and marine sediments. Montmorillonite and kaolinite are the main components of soils, which are produced by continental weathering and pedogenesis. Previous researchers have investigated the adsorption of heavy metal cations (Zn, Cu, Ni, Cd, etc.), anions (Cr, As, Se, etc.), and radionuclides (e.g., ^{137}Cs) onto clay minerals due to large surface areas and good retention ability (Manning and Goldberg, 1997; Chen et al., 1999; Gu et al., 2010; Qin et al., 2012b; Fan et al., 2014; Zhu et al., 2016; Frank et al., 2019). The reaction of clay mineral and ^{79}Se is also important to assess the mobility and environmental risks of radionuclides because ^{79}Se is an important ^{235}U fission product in the disposal of nuclear waste (e.g., Chen et al., 1999). It has been found that Ca-kaolinite and Ca-montmorillonite could adsorb Se(IV) up to 20–30 μg/g and 10–15 μg/g, respectively (Bar-Yosef and Meek, 1987; Goldberg and Glaubig, 1988). Although several studies have attempted to explore the mechanism of Se adsorption by clay minerals through X-ray absorption fine structure (XAFS) spectroscopy (e.g., Peak et al., 2006) and Triple Layer Mode (e.g., Goldberg, 2013), little is known about the relationship between the adsorption mechanism and isotope fractionation.

In this study, Se isotope fractionation during adsorption onto montmorillonite and kaolinite was clarified by combining adsorption experiments and XAFS spectroscopy. Moreover, the effects of pH and ionic strength on Se adsorption and isotope fractionation were investigated. The results would help further clarify the processes of Se adsorbed onto clay minerals and thus improve the understanding of Se isotope compositions in rocks, soils, sediments, and rivers in the supergene environment.

2. Materials and methods

2.1. Preparation of clay minerals and Se solution

Kaolinite was purchased from Hunan Xiangshui clay Co., Ltd., and montmorillonite was obtained from Inner Mongolia, China (Ma et al., 2015). Montmorillonite and kaolinite were decarbonized, and NaCl treated before the adsorption experiments. In brief, hydrogen peroxide (30% H_2O_2, superior purity) and 0.001 mol/L HCl were added to eliminate the organic matter and carbonate, respectively (Wang et al., 1999; Gu et al., 2010). Then, 0.5 mol/L NaCl to montmorillonite and 1 mol/L NaCl to the kaolinite were added and stirred for 12 h. At each step, the clay minerals were washed with 18.2 MΩ ultra-pure water for at least three times, and centrifuged at 6000 rpm for 15 min. Finally, the treated clays were freeze-dried and ground into a powder for adsorption experiments. Negligible Se was detected in the tested clay minerals by HG-AFS method after acid digestion. The clay minerals were confirmed by powder X-ray diffraction (XRD, smart lab, Cu-kα1), and the XRD data showed that the structures of clay minerals were not changed during these modification (Fig. S1).

2.2. Adsorption experiments

In this study, three series (time, ionic strength, and pH) experiments were performed to investigate the adsorption of Se(IV)/Se(VI) oxyanions onto clay minerals. Na_2SeO_3 and Na_2SeO_4 solids were purchased from Alfa Aesar (China). The solid Se reagents were dissolved in 18.2 MΩ ultra-pure water to prepare a stock solution (500 mg/L), and subpacked into 100 mL HDPE bottles. The pH of Se solutions was adjusted to designed values with 0.1 mol/L HCl or NaOH solution.

In the time-series experiment, 0.50 g montmorillonite and kaolinite were added into 50 mL centrifuge tubes containing 45 mL 0.1 mol/L NaCl solution, and the pH of suspensions was adjusted to 4.5 with 0.1 mol/L HCl or NaOH. After shaking on the oscillator for 24 h, pH was readjusted to 4.5. Then, the slurries were poured into 150 mL serum bottles and then sealed with butyl rubber plugs after purging with ultrapure nitrogen gas for 15 min to remove dissolved CO_2 and O_2. The bottle was placed on the oscillator and shaken (120 rpm) at room temperature (20 ± 2 °C), after injecting the Se(IV) or Se(VI) solution (pH = 4.5). In order to obtain enough amount of Se for accurate Se isotope measurement, Se(IV) and Se(VI) concentrations in the suspensions were set as 200 μg/L and 100 μg/L, respectively. During the experiments, 2 mL solution was sampled quickly at different time intervals after homogenizing the suspension by shaking, in order to avoid the possibe change of the liquid/solid ratio. The suspensions were filtered with 0.22-μm poly-sulfone membranes, and the filtrates were collected in 5 mL polypropylene tubes. All samples were stored in a refrigerator at 4 °C. Finally, Se concentrations in the solution were determined by the hydride generation atomic fluorescence spectrometer (HG-AFS), as described by previous studies (e.g., Zhu et al., 2008a; Qin et al., 2017b).

The ionic strength series experiment was performed under 0.01, 0.05, and 0.1 mol/L NaCl with the initial Se(IV) concentration of 200 μg/L and the pH of 4.5 for 3 days. Moreover, the effect of pH (4.5, 6, 7, and 8) on Se(IV) adsorption on clay minerals were investigated under the experimental condition of 0.01 mol/L of NaCl and 200 μg/L of Se (IV). The experimental procedure was similar to those for the time series experiments. As the affinity of clay minerals to Se(VI) was too low, the contrast experiments for ionic strength and pH were not carried out.

2.3. Sample purification

Samples were purified by the anion resin AG1-X8 to eliminate the interference of Ge and As that may be present in solution (Johnson et al., 2000). Before samples purification, double spikes (DS: ^{77}Se+^{74}Se) with known ratio was added to correct the possible isotope fractionation during purification and mass spectrometry (Zhu et al., 2008a). Briefly, samples (containing ~100 ng Se) mixed with DS were converted to Se (VI) by $K_2S_2O_8$ oxidation, then loaded onto a 1.0 ml volume AG1-X8 resin column, sequentially washed the resin with MQ water and 0.1 mol/L HCl, followed by washing with 5 mol/L HCl to elute Se(VI). Se(VI) were reduced to Se(IV) by 5 mol/L HCl at 100 °C. After cooling, Se solutions were bubbled with ultrapure N_2 for 15 min to remove the influence of volatile substances such as Br^-. Finally, the samples were diluted to (2.0 ± 0.1) mol/L HCl for isotope measurement. Detailed purification processes are described by Xu et al. (2020).

2.4. Se isotope analysis

The $\delta^{82/76}Se$ values were measured on the Nu plasma II multi-collector coupled plasma mass spectrometer (MC-ICP-MS) at the State Key Laboratory of Environmental Geochemistry, Institute of Geochemistry, Chinese Academy of Sciences, Guiyang, China, with a custom-built

hydride generation system that described in previous studies (Zhu et al., 2008a).

All $^{82/76}$Se ratios are reported as δ notation relative to NIST SRM 3149. Average external $\delta^{82/76}$Se precision was ±0.10‰ based on repeated analysis of NIST SRM 3149 standards ($n = 150$, 2SD) over three years. The long-term $\delta^{82/76}$Se values of the in-house standard MH 495 was with −3.45 ± 0.10‰ ($n = 75$, 2SD) in excellent agreement with previously reported values (Zhu et al., 2008a; Schilling et al., 2014). Meanwhile, the $\delta^{82/76}$Se values of stock solutions (Na_2SeO_3 and Na_2SeO_4) were − 1.18 ± 0.12‰ ($n = 20$, 2SD) and − 0.50 ± 0.10‰ (n = 20, 2SD), respectively.

The isotopic measurements of this study were performed on the aqueous solutions after filtration. It has been suggested that the filtration cannot lead to isotope fractionations by performing the mass budget, based on our previous results on Se adsorption on Fe oxides (Xu et al., 2020) and other elements on minerals (Barling and Anbar, 2004, Lemarchand et al., 2007, Pokrovsky et al., 2014). The long-term reproducibility (2SD) for $\delta^{82/76}$Se values of natural samples was 0.15‰. Thus, the measured Se isotope data in samples were highly reliable and robust.

Assuming that the loss of Se from the solution is solely accounted for by Se adsorption on the minerals surface and that the solids themselves were nearly Se-free, the isotopic ratio of Se adsorbed onto solid could be calculated by mass balance Eq. (1) when it reached equilibrium:

$$\delta^{82/76}Se_{adsorbed} = \left(\delta^{82/76}Se_{stock} - \delta^{82/76}Se_{dissolved} \times f\right)/(1 - f) \quad (1)$$

where $\delta^{82/76}Se_{stock}$ is the isotope ratio of the initial Se solution, $\delta^{82/76}Se_{dissolved}$ is the isotope ratios of Se in the residual solution, and f is the percentage of Se that remained in solution.

The difference in the isotopic composition of Se in solution and Se adsorbed on the solid, $\Delta^{82/76}Se_{dissolved\text{-}adsorbed}$, was calculated as:

$$\Delta^{82/76}Se_{dissolved-adsorbed} \approx \delta^{82/76}Se_{dissolved} - \delta^{82/76}Se_{adsorbed} \quad (2)$$

The estimated uncertainties on the calculated $\Delta^{82/76}Se_{dissolved\text{-}adsorbed}$ stem from Se isotope fractionation calculated by mass balance at different time interval when adsorption research equilibrium (Barling and Anbar, 2004). However, Pokrovsky et al. (2014) suggested that a lower adsorption (%) may lead to a larger calculation uncertainty. Indeed, the uncertainty of Se fractionation became very large when Se adsorption was lower than 10%, and thus Se isotope fractionation data for the experiments with <10% adsorption were not calculated and discussed in this study.

2.5. XAFS measurement and data analysis

Selenium K-edge XAFS spectra of Se(IV)-adsorbed samples were obtained at the BL14W1 beamline of the Shanghai Synchrotron Radiation Facility (SSRF, Shanghai, China) and the beamline BL12C at the Photon Factory, KEK (Tsukuba, Japan). The X-rays were monochromatized with a pair of Si(111) crystals. Energy calibration was performed using $NaHSeO_3$ by defining the energy of 12.658 keV at the maximum peak of white line. The adsorbed samples were placed at an angle of 45° from the incident beam to record Se EXAFS spectra in fluorescence mode using a Ge solid-state detector (SSD) under the ambient condition. The solid Se-adsorbed montmorillonite and kaolinite were separated from the final suspension with a membrane filter (0.22 μm) after adsorption equilibration, and then washed with MQ water and packed into a polyethylene bag. In the present study, the Se(IV) adsorbed samples prepared at pH 4.5 were selected to obtain enough quality EXAFS spectra because of the high adsorption. Repeated scans were carried out to improve the quality, and no radiation damage was found for the adsorbed sample during data acquisition.

The XAFS spectra were analyzed using the REX2000 software (Rigaku Co. Ltd.) and FEFF 7.02. The $k^3\chi(k)$ oscillation was extracted and Fourier transformed to get radial structural function (RSF) after removing the background of XAFS spectra. The RSF was simulated using the curve-fitting method to obtain structural parameters. The quality of the fitting was given by the goodness of fit parameter, R factor, defined as:

$$R = \sum \left\{k^3 x_{obs}(k) - k^3 x_{cal}(k)\right\}^2 \Big/ \sum \left\{k^3 x_{obs}(k)\right\}^2 \quad (3)$$

where $\chi_{cal}(k)$ and $\chi_{obs}(k)$ are the calculated and experimental absorption coefficients at a given wavenumber (k), respectively. Details of the XAFS measurement and analysis are similar to those described in the previous studies (e.g., Qin et al., 2019, 2020).

3. Results

3.1. Se adsorption behavior of clay minerals

The kinetic results showed that the adsorption equilibrium was nearly reached after 48 h for Se(IV) adsorption onto montmorillonite and kaolinite, while that for Se(VI) adsorption was less than 24 h (Fig. 1). The maximum amounts of Se(IV) adsorbed onto the two clay minerals were larger in comparison with Se(VI) adsorption. The adsorption of Se(IV) onto montmorillonite and kaolinite (pH 4.5) were ~ 23% and ~ 19%, respectively. By contrast, much smaller adsorptions (< 4%) were found for Se(VI) on these minerals. The adsorption of Se oxyanions by clay minerals is much lower than those for other minerals (e.g., Fe oxides), which could be ascribed to the permanent negative structural charge and low point of zero charge for clay minerals.

The adsorption of Se(IV) onto kaolinite at 0.01 mol/L and 0.05 mol/L NaCl showed similar trends, but decreased at higher ionic strength (0.1 mol/L NaCl). By contrast, the adsorption of Se(IV) onto montmorillonite was almost not affected by ionic strength. In addition, the adsorption of Se(IV) decreased with increasing pH (4.5–8) for montmorillonite, whereas the adsorption of Se(IV) by kaolinite increased at low pH (≤ 6) but decreased at higher pH (> 6) (Table 1).

3.2. Se isotope fractionation during Se(VI)/Se(IV) oxyanions adsorption onto clay minerals

In the experiments of Se(VI) adsorption onto montmorillonite and kaolinite, Se isotope values ($\delta^{82/76}$Se) in solution did not obviously change over time and were close to the value of stock solution (−0.50 ± 0.10‰), indicating that there was little or no Se isotope fractionation (Fig. 2). By contrast, it was obviously found that the values of $\delta^{82/76}$Se (IV) in solution increased firstly and then decreased slowly to the initial value for montmorillonite and kaolinite in particular at higher ionic strength (Fig. 2). The Se isotope variation was up to 0.30‰ during the adsorption of Se(IV) onto kaolinite at pH 4.5 with 0.1 mol/L NaCl (Fig. 2). Interestingly, Se(IV) isotope fractionation appeared to not be significant affected by the different pH (4.5–8) examined in this study (Table 1).

Interestingly, the variations of Se isotope was slightly different between Se(IV) adsorption onto montmorillonite and kaolinite as a function of ionic strength (Fig. 2). In the case of kaolinite at pH 4.5, Se(IV) isotope fractionation reached equilibrium after ~72 h, and the values of $\delta^{82/76}$Se(IV) in solution increased slightly at the initial stage and were finally close to the stock value. According to mass balance Eqs. (1) and (2), the difference of Se isotope fractionations ($\Delta^{82/76}Se_{dissolved\text{-}adsorbed}$) between solution and solid after 72 h were calculated to be 0.15 ± 0.14‰ ($n = 3$, 2SD), 0.21 ± 0.17‰ (n = 3, 2SD), and 0.23 ± 0.19‰ (n = 3, 2SD) at 0.01, 0.05, and 0.1 mol/L of NaCl, respectively. By comparison, the $\Delta^{82/76}Se_{dissolved\text{-}adsorbed}$ values for montmorillonite adsorption at pH 4.5 after 72 h were 0.19 ± 0.14‰ (n = 3, 2SD), 0.01 ± 0.14‰ (n = 3, 2SD), and 0.18 ± 0.12‰ (n = 3, 2SD) at 0.01, 0.05, and 0.1 mol/L NaCl, respectively.

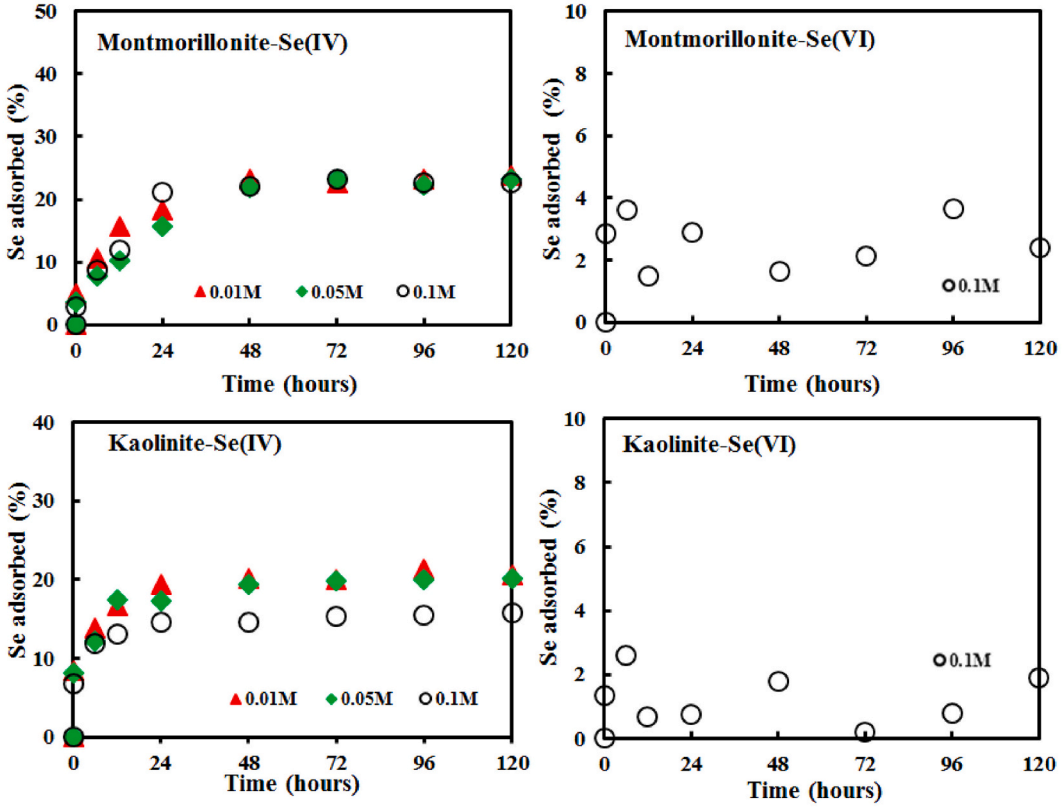

Fig. 1. Adsorption of Se onto clay minerals as a function of time (hours) at pH 4.5.

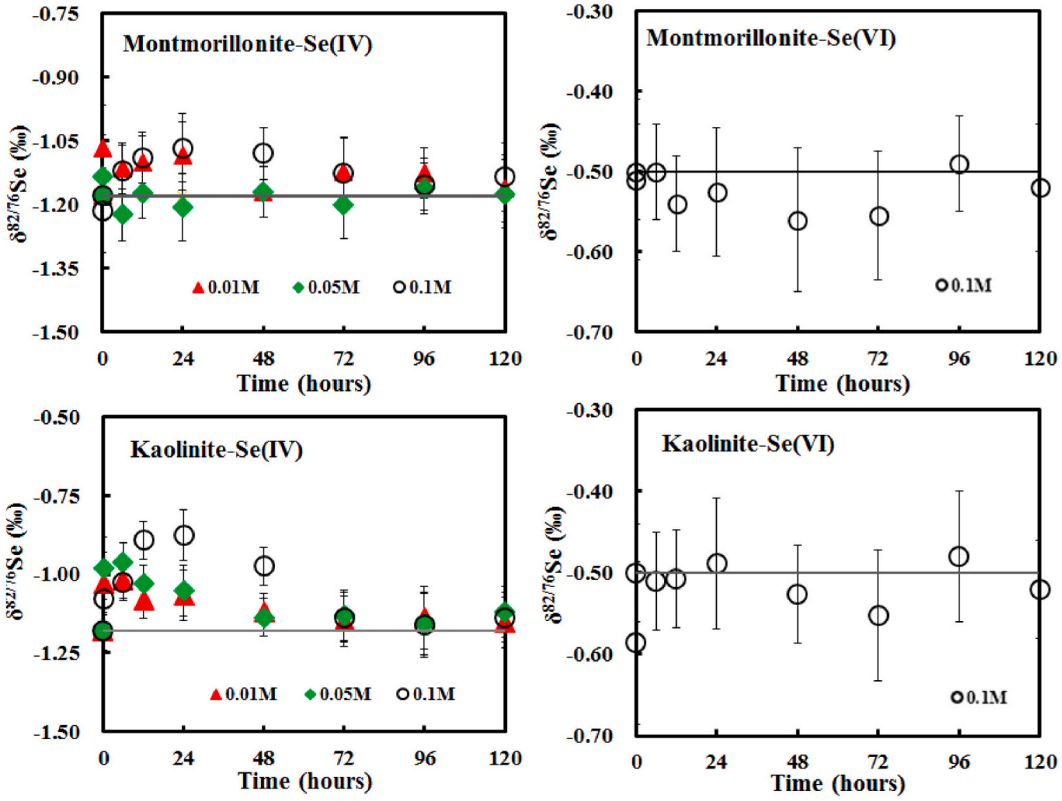

Fig. 2. The $\delta^{82/76}$Se values of the solution during adsorption onto clay minerals as a function time (hours) at pH 4.5. Black lines represent the $\delta^{82/76}$Se values of the stock solutions.

Table 1
Se isotope fractionation during Se(IV) adsorption onto clay minerals at different pH.

Adsorbents	pH	C_e (μg/L)	Q_e (ug/g)	Se adsorbed (%)	f	$\delta^{82/76}Se_{dissolved}$	$\delta^{82/76}Se_{adsorbed}$	$\Delta^{82/76}Se_{dissolved\text{-}adsorbed}$	2SD of Δ
Montmorillonite	4.5	152.54	4.75	23.73	0.76	−1.14	−1.32	0.19	0.14
	6.0	168.22	3.18	15.89	0.84	−1.15	−1.35	0.21	0.15
	7.0	180.61	1.94	9.70	0.90	−1.16	−1.38	0.23	0.15
	8.0*	186.58	1.34	6.71	0.93	−1.19	−1.03	–	–
Kaolinite	4.5	168.48	3.15	15.76	0.84	−1.16	−1.31	0.15	0.14
	6.0	144.26	5.57	27.87	0.72	−1.13	−1.32	0.19	0.14
	7.0	149.66	5.03	25.17	0.75	−1.15	−1.27	0.12	0.14
	8.0*	185.78	1.42	7.11	0.93	−1.16	−1.38	–	–

C_e and Q_e represent the equilibrium concentration and adsorption capacity, $Q_e = (C_0 - C_e)*V/m$, V is the volume of the solution, and m is the mass of the adsorbent. f represents the fraction of Se remaining in solution. * $\Delta^{82/76}Se_{dissolved\text{-}adsorbed}$ was not calculated because of the low Se adsorption rate.

3.3. Se K-edge XAFS analysis

Fig. 3 shows the X-ray absorption near edge structure (XANES) spectra for Se(IV)-adsorbed montmorillonite and kaolinite. It was found that the peak energies of the XANES spectra for the two samples were essentially identical to that for aqueous Se(IV) solution at pH 4.5 (mainly $HSeO_3^-$ species, Séby et al., 2001), suggesting that the oxidation state of Se does not change during Se(IV) adsorption onto clay minerals under the experimental conditions.

Furthermore, the $k^3\chi(k)$ spectra and RSF of Se(IV)-adsorbed materials were also very similar to those for Se(IV) solution. The EXAFS analysis showed that there was only one prominent peak assigned to Se-O shell in the RSFs of adsorbed samples, with the absence of distant peaks that may be contributed from other shells (e.g., Se-Si, Se-Al, or Se-Fe shells) (Fig. 4 and Table 2). The quantitative results obtained by the curve-fitting analysis showed that the pronounced peaks around R + ΔR = 1.2 Å (phase shift not corrected) for montmorillonite and kaolinite were assigned to the Se-O shell at 1.68–1.69 Å, which is consistent with that for Se(IV) solution (Table 2). Thus, the appearance of only Se-O shell and the absences of other distant shells obtained from Se K-edge EXAFS analysis strongly indicate that Se is mainly adsorbed on montmorillonite and kaolinite at pH 4.5 via the outer-sphere complexation.

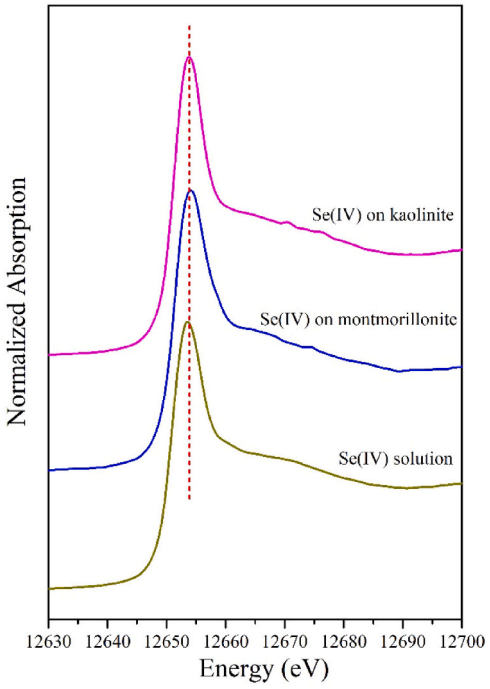

Fig. 3. Se K-edge XANES spectra for aqueous Se(IV) solution (pH 4.5), Se(IV)-adsorbed montmorillonite and kaolinite.

4. Discussion

4.1. The effect of pH on Se adsorption and isotope fractionation for clay minerals

Previous studies indicated that the adsorption of anions gradually decreases with the increasing pH (e.g., Weerasooriya et al., 1998; Missana et al., 2009). This trend was also observed for Se(IV) adsorption onto montmorillonite examined in the present study (Table 1). This phenomenon may be due to the low point of net zero charge (pH_{PZC}) of montmorillonite (4.4–5.5) (Saha et al., 2004; Duc et al., 2006). The higher experimental pH (4.5–8) in this study may result in more negative charges on the montmorillonite surface, and thus the adsorption of negatively-charged Se(IV) species (e.g., SeO_3^{2-} or $HSeO_3^-$) would decrease because of larger electrostatic repulsion at higher pH condition.

For kaolinite, Se(IV) adsorption increased under the lower pH (<7) but decreased under alkaline conditions, which is similar to the observation by Goldberg and Glaubig (1988). This may be related to the charges of siloxanol and aluminol surfaces on kaolinite. Spark et al. (1995) considered that the edges and alumina surface of kaolinite would become negatively-charged when the pH is above the pH_{PZC} of the aluminol groups (pH_{PZC} = 7.2), although the kaolinite surface is generally positively charged under acidic conditions (pH <7.2). In combination with the greater proportion of edge surface area for kaolinite (Goldberg and Glaubig, 1988), this specific physic-chemical property of kaolinite could be used to explain the roughly twice adsorption for Se(IV) on kaolinite at pH 6–7 compared with montmorillonite (Table 1).

However, there was no obvious difference between the isotope compositions of Se in solution and clay minerals under different pH at adsorption equilibrium, which is different from the influence of pH on the amount of Se on montmorillonite and kaolinite. The exceptional case for montmorillonite at pH 8 may be ascribed to a larger calculation error caused by the low Se adsorption. By contrast, several studies showed that pH could affect isotopic fractionation of some elements (e.g., Zn and Mo) under some conditions (e.g., Juillot et al., 2008; Goldberg et al., 2009). Goldberg et al. (2009) observed the larger Mo isotope fractionation ($\Delta^{98}Mo$) during adsorption onto Fe oxides at a higher pH. They speculated that the most isotopically-depleted Mo species (e.g., MoO_3 relative to $MoO_3(H_2O)_3$ and other intermediates) were preferentially adsorbed by Fe oxides at higher pH, resulting in a relative larger Mo isotope fractionation at higher pH.

In the case of Se, it has been suggested by the Triple-Layer model that the surface speciation of Se(IV) adsorption on kaolinite was mainly as SOH_2-$HSeO_3^-$ (≥60%) when pH ≤ 6 while as SOH_2^+-SeO_3^{2-} when pH >6 (≥ 60%) (Goldberg, 2013). Nonetheless, Se isotope fractionations caused by adsorption on clay minerals were not significantly related to the species of Se(IV) under the experimental conditions, which is consistent with the previous research regarding the adsorption of Se oxyanions by Fe/Mn/Al oxides (e.g., Xu et al., 2020). Similarly, Pokrovsky et al. (2014) indicated that the pH has a little effect on the isotope

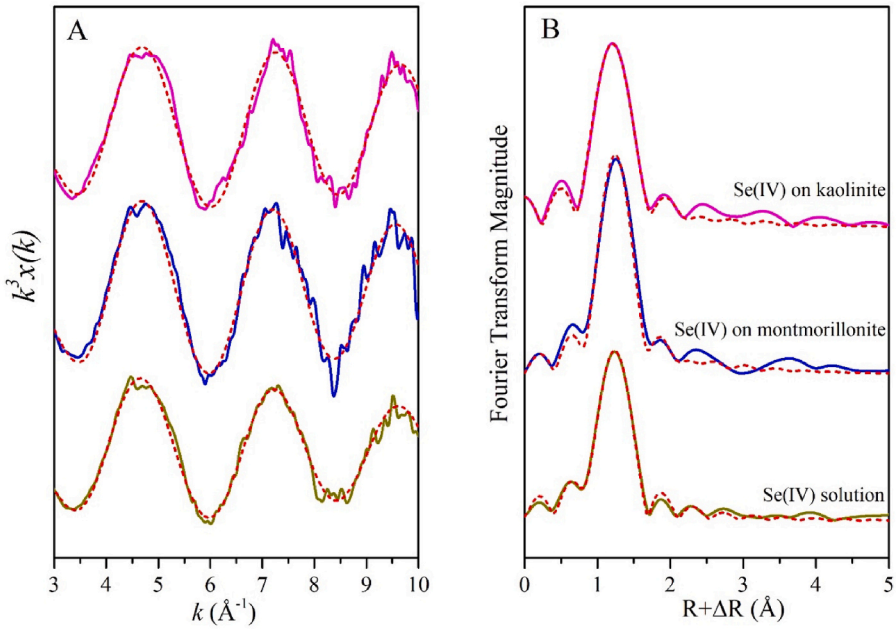

Fig. 4. Se K-edge EXAFS spectra for aqueous Se(IV) solution, Se(IV)-adsorbed montmorillonite and kaolinite (A: k^3-weighted $x(k)$ spectra; B: RSFs (phase shift not corrected)). Solid lines are spectra obtained by experiments, and red dash lines are calculated spectra by a curve-fitting analysis.

Table 2
Structural parameters of Se-adsorbed clay minerals obtained by a curve-fitting analysis of Se K-edge EXAFS spectra.

Sample	Shell	CN	R (Å)	ΔE_0 (eV)	σ^2 (Å^2)	R factor
Se(IV) solution	Se-O	2.6 (3)	1.68 (1)	7(2)	0.003 (1)	0.03
Se(IV) on montmorillonite	Se-O	2.8 (3)	1.69 (2)	9(2)	0.002 (1)	0.11
Se(IV) on kaolinite	Se-O	2.8 (4)	1.68 (1)	7(2)	0.002 (1)	0.51

CN: coordination number; R: interatomic distance; ΔE_0: threshold E_0 shift; σ^2: Debye-Waller factor.
The uncertainties in the last digit are reported in parentheses.

fractionation of Ge during adsorption on goethite, and proposed that the degree of protonation of $Ge(O, OH)_4$ tetrahedra at the goethite surface does not impact Ge isotopic fractionation between aqueous solution and the goethite surface. Considering that dissolved Se(IV) mainly exists as $HSeO_3^-$ (> 95%) species at a wide range of pH (Séby et al., 2001), the protonation degree of Se adsorbed on the surfaces of clay minerals is not the main cause for Se isotope fractionation between the aqueous and adsorbed phases during adsorption on clay minerals.

4.2. Comparison of Se isotope fractionation during adsorption onto montmorillonite and kaolinite

The $\delta^{82/76}$Se values in solution varied over time during Se(IV) adsorption onto clay minerals, but those were mostly close to the $\delta^{82/76}$Se value of stock solution after ~72 h. The increase of $\delta^{82/76}$Se values in solution in the first 3 h may reflect that a kinetic effect largely governs the observed Se fractionation due to the fast sorption of isotopically lighter Se, while the decreased $\delta^{82/76}$Se values in solution over the time (after the first 3 h) may imply that Se fractionation is mainly controlled by isotopes exchange between adsorbed and dissolved Se, as suggested by several studies for other elements (Ellis, 2003; Wasylenki et al., 2014). The calculated Se isotope fractionations ($\Delta^{82/76}Se_{dissolved\text{-}adsorbed}$) were $\leq$ 0.23‰, suggesting an insignificant enrichment of lighter Se isotopes on the mineral surfaces during adsorption of Se onto clay minerals.

Moreover, the $\delta^{82/76}$Se values in solution increased firstly and then decreased during Se(IV) adsorption onto kaolinite, which was consistent with Se(IV) adsorption onto Al oxides (Xu et al., 2020). By contrast, this phenomenon was not clearly observed for montmorillonite. This different behavior of Se isotope fractionation between the two clay minerals may be related to the structure of kaolinite and montmorillonite, because the adsorption of Se oxyanions by clay minerals were mainly through aluminol sites (≡Al-OH) (Peak et al., 2006). Montmorillonite is a 2:1 layer phyllosilicate mineral, and its alumina octahedron is located between two silica tetrahedrons, while kaolinite is a 1:1 layer mineral, with its alumina octahedron and silica tetrahedron being arranged in parallel (Brigatti et al., 2006). Thus, the interaction of Se(IV) oxyanion with the aluminol sites in kaolinite may be more ready compared with those in montmorillonite (Bar-Yosef and Meek, 1987).

In addition, the adsorption of Se(IV) on kaolinite was affected by ionic strength with the larger Se isotope variation in solution at the higher ionic strength, whereas this influence was not obvious for montmorillonite (Fig. 2). This may also be explained by the fact that the aluminol group in the structure of kaolinite (1:1 layer) is more likely to be affected by pH and ionic strength (Bar-Yosef and Meek, 1987; Goldberg and Glaubig, 1988; Manning and Goldberg, 1997). Previous studies observed a similar influence by the ionic strength for Zn and Cd adsorption onto oxides and clay minerals and speculated that the cause might be related to Zn and Cd species at different ionic strengths (e.g., Wasylenki et al., 2014; Bryan et al., 2015). However, the main species of Se(IV) was $HSeO_3^{2-}$ (>99.5%) at 0.01–0.1 mol/L NaCl and pH 4.5 according to Visual MINTEQ 3.0, which likely suggests that the effect of ionic strength on Se isotope fractionation for Se(IV) onto kaolinite is not related to Se species.

4.3. Possible mechanism for Se isotope fractionation during adsorption onto clay minerals

Previous studies indicated that Se was adsorbed onto clay minerals via electrostatic adsorption or colloidal complexation (e.g., Bar-Yosef and Meek, 1987; Goldberg and Glaubig, 1988). Bickmore et al. (2003) and Tournassat et al. (2004) considered that silanol (≡Si-OH), aluminol (≡Al–OH), silica-alumina bridging sites (≡SiAl–OH), and alumina-

alumina bridging sites (≡Al_2–OH) can contribute to the proton bonding at clay minerals edge surface. Weerasooriya et al. (1998) indicated that only aluminol and silanol at the edge surface was helpful to the proton bonding. Further, Bourg et al. (2007) proposed that ≡Al_2–OH site was probably the most important adsorption site at the pH range of 4.5–9. In terms of montmorillonite and kaolinite, a small amount of positive variable charges (≡S–OH_2^+) generated from the protonation of minerals edge sites (Manning and Goldberg, 1997; Gu et al., 2010), which could adsorb negatively charged Se oxyanions via electrostatic adsorption. Moreover, the adsorption experiments of Se oxyanions on quartz showed that the adsorption was very low and Se isotope ratio in the solution had almost no change during adsorption, which suggests that the silanol sites in clay minerals may not largely affect Se adsorption and isotope under experimental conditions in this study. Accordingly, it could be expected that small Se isotope fractionations during adsorption on clay minerals are mainly controlled by the ≡Al-OH sites.

Furthermore, it has been demonstrated that the isotope fractionation of an element can be related to the structures of the surface complex formed on the minerals, as reported for B (Lemarchand et al., 2007), Ge (Li and Liu, 2010; Pokrovsky et al., 2014), Mo (Kashiwabara et al., 2011) and W (Kashiwabara et al., 2017). By analogy, Se isotope fractionation could be also governed by the surface complexation during adsorption onto clay minerals. In the present study, Se K-edge EXAFS results showed that Se(IV) is mostly adsorbed on montmorillonite and kaolinite via the weak outer-sphere complexation under experimental conditions. Similarly, Goldberg (2013) found that Se(IV) is mainly adsorbed onto montmorillonite and kaolinite with the formation of outer-sphere complexes through the Three-Layer model. However, Peak et al. (2006) indicated that Se(IV) forms a bidentate binuclear inner-sphere complex on pure montmorillonite based on Se K-edge XANES and EXAFS results. This disparity may be attributed to the different montmorillonite mineral and experimental conditions. It is possible that natural montmorillonite used in Peak's study contain other elements (e.g., Fe and Mn) that may have an influence on the adsorption of negatively-charged oxyanions by clay minerals (Brigatti et al., 2006; Frank et al., 2019). Another possible reason for the difference may be ascribed to the hydrolysis of Al oxides in the clay minerals, because the active Al oxides probably undergone hydrolysis or aging in solution (Catalano et al., 2006a). In the case of this study, the longer adsorption time may imply more strong hydrolysis of the functional group (≡Al-OH) of the clay minerals. As a result, the outer-sphere complexes can be preferentially formed on the clay mineral, and the possible inner-sphere complexes would be transformed with the hydrolysis of functional group, even if the inner-sphere complexes with Al-OH might be formed at the initial period.

The results show that Se isotope fractionation during Se(IV) adsorbed on montmorillonite and kaolinite was very small, with the $\Delta^{82/76}Se_{dissolved\text{-}adsorbed}$ values of 0.12–0.23‰ (Table 1). These results were comparable to that for Se(IV) isotope fractionation caused by adsorption on Al oxides (≤ 0.20‰), for which the outer-sphere complexation may be the main adsorption mechanism (Xu et al., 2020). Furthermore, the $\Delta^{82/76}Se_{dissolved\text{-}adsorbed}$ values for clay minerals were much lower compared with Fe and Mn oxides that have a great affinity for Se(IV) because of the inner-sphere complexation (Balistrieri and Chao, 1990; Catalano et al., 2006b). Therefore, the mechanism for little or no Se isotope fractionation during adsorption on clay minerals is likely related to the formation of dominant outer-sphere complexes on the mineral surfaces, as revealed by the EXAFS analysis in this study.

4.4. Implications

Montmorillonite and kaolinite are the major secondary minerals in soils produced during continental weathering and pedogenesis, as well as the major components of deep-sea sediments, which may influence Se geochemical cycling through the adsorption process (Bar-Yosef and Meek, 1987; Goldberg and Glaubig, 1988; Missana et al., 2009; Goldberg, 2013). This study showed an insignificant Se isotope fractionation during Se adsorption onto the surface of montmorillonite and kaolinite. The results imply that Se isotopes are still effective for constraining redox conditions in both modern and ancient environments and tracing the continental weathering processes in highly weathered environments where Fe/Mn/Al oxides and clays are abundant.

It has been demonstrated that abiotic redox (e.g., Johnson and Bullen, 2003), biomethylation (Schilling et al., 2013), and biological processes (e.g., Herbel et al., 2000) could cause significant Se isotope fractionations (>1.5‰), while other processes such as precipitation, volatilization, oxidation, and adsorption resulted in relatively smaller Se isotope fractionations (< 1.5‰) (e.g., Johnson et al., 1999; Mitchell et al., 2013; Xu et al., 2020). In most cases, variations of Se isotopic ratios result from more than one process in natural soil and sediment environments, where complex processes such as redox changes, rock/water interaction, and biologic activity may occur. For example, several studies showed large ranges of Se isotope compositions ($\delta^{82/76}Se$) in the soils (−3.05‰-1.33‰) and deep-sea sediments (−1.09‰- 3.90‰) (e.g., Rouxel et al., 2002; Schilling et al., 2011; Mitchell et al., 2013; Zhu et al., 2014), which were significantly greater than Se isotope fractionation induced by Se oxyanions adsorption onto Fe/Mn/Al oxides and clay minerals (<1.50‰) (e.g., Johnson et al., 1999; Mitchell et al., 2013; Xu et al., 2020). These results further verify that the larger Se isotope variations in highly weathered environments are mainly affected by biologic or abiotic reduction other than adsorption processes.

5. Conclusions

This study firstly reports Se isotope fractionation during Se oxyanions adsorption onto montmorillonite and kaolinite. Results show that Se isotope fractionations caused by Se(IV) adsorption onto montmorillonite and kaolinite are insignificant ($\Delta^{82/76}Se_{dissolved\text{-}adsorbed} \leq 0.23‰$), while almost no Se isotope fractionation is observed for Se(VI) adsorption onto the two clay minerals. In combination with adsorption experiments and EXAFS analysis, the outer-sphere complexation could be the dominant mechanism controlling Se isotope fractionation during adsorption onto montmorillonite and kaolinite. The findings from this study provide the molecular evidence for the mechanism of Se isotope fractionation during adsorption onto clay minerals, which would help understand the variations of Se isotope signals in the natural environment.

Declaration of Competing Interest

The authors declare that they have no known competing financial interests or personal relationships that could have appeared to influence the work reported in this paper.

Acknowledgements

This research was supported by the National Natural Science Foundation of China (Nos. U1732132, 41273029, and 41473028). The authors thank Prof. Hongping He from Guangzhou Institute of Geochemistry, Chinese Academy of Sciences for providing montmorillonite, and Dr. Liang Liang, Kai Lu, Bo Zhao for their assistance with the sample preparation, as well as Dr. Jing Wang and Dr. Li Zeng for assistance with mass spectrometry.

Appendix A. Supplementary data

Supplementary data to this article can be found online at https://doi.org/10.1016/j.clay.2021.106189.

References

Balistrieri, L.S., Chao, T.T., 1990. Adsorption of selenium by amorphous iron oxyhydroxide and manganese dioxide. Geochim. Cosmochim. Acta 54, 739–751.

Barling, J, Anbar, A.D., 2004. Molybdenum isotope fractionation during adsorption by manganese oxides. Earth Planet. Sci. Lett. 217, 315–329.

Bar-Yosef, B., Meek, D., 1987. Selenium sorption by Kaolinite and Montmorillonite. Soil Sci. 144, 11–19.

Bickmore, B.R., Rosso, K.M., Nagy, K.L., Cygan, R.T., Tadanier, C.J., 2003. Ab initio determination of edge surface structures for dioctahedral 2:1 phyllosilicates: implications for acid-base reactivity. Clay Clay Miner. 51, 359–371.

Bourg, I.C., Sposito, G., Bourg, A.C., 2007. Modeling the acid-base surface chemistry of montmorillonite. J. Colloid Interface Sci. 312, 297–310.

Brigatti, M.F., Galan, E., Theng, B.K.G., 2006. Structures and Mineralogy of Clay Minerals. Dev. Clay Sci. 1, 19–86.

Bryan, A.L., Dong, S., Wilkes, E.B., Wasylenki, L.E., 2015. Zinc isotope fractionation during adsorption onto Mn oxyhydroxide at low and high ionic strength. Geochim. Cosmochim. Acta 157, 182–197.

Catalano, J.G., Park, C., Zhang, Z., Fenter, P., 2006a. Termination and water adsorption at the α-Al_2O_3 (012)-aqueous solution interface. Langmuir 22, 4668–4673.

Catalano, J.G., Zhang, Z., Fenter, P., Bedzyk, M.J., 2006b. Inner-sphere adsorption geometry of Se(IV) at the hematite (100)-water interface. J. Colloid Interface Sci. 297, 665–671.

Chang, Y., Zhang, J., Qu, J.-Q., Xue, Y., 2017. Precise selenium isotope measurement in seawater by carbon-containing hydride generation-desolvation-MC-ICP-MS after thiol resin preconcentration. Chem. Geol. 471, 65–73.

Chen, F., Burns, P.C., Ewing, R.C., 1999. ^{79}Se: geochemical and crystallo-chemical retardation mechanisms. J. Nucl. Mater. 275, 81–94.

Clark, S.K., Johnson, T.M., 2010. Selenium stable isotope investigation into selenium biogeochemical cycling in a lacustrine environment: Sweitzer Lake. Colorado. J. Environ. Qual. 39, 2200–2210.

Duc, M., Thomas, F., Gaboriaud, F., 2006. Coupled chemical processes at clay/electrolyte interface: a batch titration study of Na-montmorillonites. J. Colloid Interface Sci. 300, 616–625.

Ellis, A., 2003. Selenium and Chromium Stable Isotopes and the Fate of Redox-Active Contaminants in the Environment Ph.D. thesis. The University of Illinois at Urbana-Champain, Urbana, Illinois.

Elrashidi, M.A., Adriano, D.C., Workman, S.M., Lindsay, W.L., 1987. Chemical Equilibria of Selenium in Soils. Soil Sci. 144, 141–152.

Fan, Q.H., Tanaka, M., Tanaka, K., Sakaguchi, A., Takahashi, Y., 2014. An EXAFS study on the effects of natural organic matter and the expandability of clay minerals on cesium adsorption and mobility. Geochim. Cosmochim. Acta 135, 49–65.

Fordyce, F.M., 2013. Selenium deficiency and toxicity in the environment. In: Selinus, O. (Ed.), Essentials of Medical Geology. Springer, Dordrecht, pp. 375–416.

Francisco, P.C.M., Sato, T., Otake, T., Kasama, T., Suzuki, S., Shiwaku, H., Yaita, T., 2018. Mechanisms of Se(IV) co-precipitation with ferrihydrite at acidic and alkaline conditions and its behavior during aging. Environ. Sci. Technol. 52, 4817–4826.

Frank, A.B., Klaebe, R.M., Frei, R., 2019. Fractionation behavior of chromium isotopes during the sorption of Cr(VI) on kaolin and its implications for using black shales as a paleoredox archive. Geochem. Geophys. Geosyst. 20, 2290–2302.

Goldberg, S., 2013. Modeling selenite adsorption envelopes on oxides, clay minerals, and soils using the triple layer model. Soil Sci. Soc. Am. J. 77, 64–71.

Goldberg, S., Glaubig, R.A., 1988. Anion sorption on a calcareous, montmorillonitic soil-selenium. Soil Sci. Soc. Am. J. 54, 954–958.

Goldberg, T., Archer, C., Vance, D., Poulton, S.W., 2009. Mo isotope fractionation during adsorption to Fe (oxyhydr)oxides. Geochim. Cosmochim. Acta 73, 6502–6516.

Gu, X., Evans, L.J., Barabash, S.J., 2010. Modeling the adsorption of Cd (II), Cu (II), Ni (II), Pb (II) and Zn (II) onto montmorillonite. Geochim. Cosmochim. Acta 74, 5718–5728.

Herbel, M.J., Johnson, T.M., Oremland, R.S., Bullen, T.D., 2000. Fractionation of selenium isotopes during bacterial respiratory reduction of selenium oxyanions. Geochim. Cosmochim. Acta 64, 3701–3709.

Johnson, T.M., Bullen, T.D., 2003. Selenium isotope fractionation during reduction by Fe (II)-Fe(III) hydroxide-sulfate (green rust). Geochim. Cosmochim. Acta 67, 413–419.

Johnson, T.M., Herbel, M.J., Bullen, T.D., Zawislanski, P.T., 1999. Selenium isotope ratios as indicators of selenium sources and oxyanion reduction. Geochim. Cosmochim. Acta 63 (18), 2775–2783.

Johnson, T.M., Bullen, T.D., Zawislanski, P.T., 2000. Selenium Stable Isotope Ratios as Indicators of sources and Cycling of Selenium results from the Northern Reach of San Francisco Bay. Environ. Sci. Technol. 34, 2075–2079.

Juillot, F.C., Marechal, C., Ponthieu, M., Cacaly, S., Morin, G., Benedetti, M., Hazemann, J.L., Proux, O., Guyot, F., 2008. Zn isotopic fractionation caused by sorption on goethite and 2-Lines ferrihydrite. Geochim. Cosmochim. Acta 72, 4886–4900.

Kashiwabara, T., Takahashi, Y., Tanimizu, M., Usui, A., 2011. Molecular-scale mechanisms of distribution and isotopic fractionation of molybdenum between seawater and ferromanganese oxides. Geochim. Cosmochim. Acta 75, 5762–5784.

Kashiwabara, T., Kubo, S., Tanaka, M., Senda, R., Iizuka, T., Tanimizu, M., Takahashi, Y., 2017. Stable isotope fractionation of tungsten during adsorption on Fe and Mn (oxyhydr)oxides. Geochim. Cosmochim. Acta 204, 52–67.

Kipp, M.A., Stueken, E.E., Bekker, A., Buick, R., 2017. Selenium isotopes record extensive marine suboxia during the great oxidation event. Proc. Natl. Acad. Sci. U. S. A. 114, 875–880.

Lemarchand, E., Schott, J., Gaillardet, J., 2007. How surface complexes impact boron isotope fractionation: evidence from Fe and Mn oxides sorption experiments. Earth Planet. Sci. Lett. 260, 277–296.

Li, X.F., Liu, Y., 2010. First-principles study of Ge isotope fractionation during adsorption on Fe(III)-oxyhydroxide surfaces. Chem. Geol. 278, 15–22.

Ma, L.Y., Zhu, J.X., Xi, Y.F., Zhu, R.L., He, H., Liang, P., Ayoko, X.L., G.A, 2015. Simultaneous adsorption of Cd(II) and phosphate on Al_{13} pillared montmorillonite. RSC Adv. 5, 77227–77234.

Manning, B.A., Goldberg, S., 1997. Adsorption and stability of arsenic(III) at the clay mineral–water interface. Environ. Sci. Technol. 31, 2005–2011.

Missana, T., Alonso, U., Garcia-Gutierrez, M., 2009. Experimental study and modelling of selenite sorption onto illite and smectite clays. J. Colloid Interface Sci. 334, 132–138.

Mitchell, K., Mason, P.R.D., Van Cappellen, P., Johnson, T.M., Gill, B.C., Owens, J.D., Diaz, J., Ingall, E.D., Reichart, G.-J., Lyons, T.W., 2012. Selenium as paleo-oceanographic proxy: a first assessment. Geochim. Cosmochim. Acta 89, 302–317.

Mitchell, K., Couture, R.-M., Johnson, T.M., Mason, P.R.D., Van Cappellen, P., 2013. Selenium sorption and isotope fractionation: Iron(III) oxides versus iron(II) sulfides. Chem. Geol. 342, 21–28.

Peak, D., Saha, U.K., Huang, P.M., 2006. Selenite adsorption mechanisms on pure and coated montmorillonite an EXAFS and XANES spectroscopic study. Soil Sci. Soc. Am. J. 70, 192–203.

Pogge von Strandmann, P.A.E., Stüeken, E.E., Elliott, T., Poulton, S.W., Dehler, C.M., Canfield, D.E., Catling, D.C., 2015. Selenium isotope evidence for progressive oxidation of the Neoproterozoic biosphere. Nat. Commun. 6, 1–10.

Pokrovsky, O.S., Galy, A., Schott, J., Pokrovski, G.S., Mantoura, S., 2014. Germanium isotope fractionation during Ge adsorption on goethite and its coprecipitation with Fe oxy(hydr)oxides. Geochim. Cosmochim. Acta 131, 138–149.

Qin, H.B., Yokoyama, Y., Fan, Q.H., Iwatani, H., Tanaka, K., Sakaguchi, A., Kanai, Y., Zhu, J.M., Onda, Y., Takahashi, Y., 2012b. Investigation of cesium adsorption on soil and sediment samples from Fukushima Prefecture by sequential extraction and EXAFS technique. Geochem. J. 46, 297–302.

Qin, H.B., Zhu, J.M., Liang, L., Wang, M.S., Su, H., 2013. The bioavailability of selenium and risk assessment for human selenium poisoning in high-Se areas. China. Environ. Int. 52, 66–74.

Qin, H.B., Takeichi, Y., Nitani, H., Terada, Y., Takahashi, Y., 2017a. Tellurium distribution and speciation in contaminated soils from abandoned mine tailings: comparison with selenium. Environ. Sci. Technol. 51, 6027–6035.

Qin, H.B., Zhu, J.M., Lin, Z.Q., Xu, W.P., Tan, D.C., Zheng, L.R., Takahashi, Y., 2017b. Selenium speciation in seleniferous agricultural soils under differen cropping systems using sequential extraction and X-ray absorption spectroscopy. Environ. Pollut. 225, 361–369.

Qin, H.B., Uesugi, S., Yang, S.T., Tanaka, M., Kashiwabara, T., Itai, T., Usui, A., Takahashi, Y., 2019. Enrichment mechanisms of antimony and arsenic in marine ferromanganese oxides: insights from the structural similarity. Geochim. Cosmochim. Acta 257, 110–130.

Qin, H.B., Yang, S.T., Tanaka, M., Sanematsu, K., Arcilla, C., Takahashi, Y., 2020. Chemical speciation of scandium and yttrium in laterites: new insights into the control of their partitioning behaviors. Chem. Geol. 552, 119771.

Qin, H.B., Zhu, J.M., Su, H., 2012a. Selenium fractions in organic matter from Se-rich soils and weathered stone coal in selenosis areas of China. Chemosphere 86, 626–633.

Rouxel, O., Ludden, J., Carignan, J., Marin, L., Fouquet, Y., 2002. Natural variations of Se isotopic composition determined by hydride generation multiple collector inductively coupled plasma mass spectrometry. Geochim. Cosmochim. Acta 66, 3191–3199.

Saha, U.K., Liu, C., Kozak, L.M., Huang, P.M., 2004. Kinetics of selenite adsorption on hydroxyaluminum- and hydroxyaluminosilicate-montmorillonite complexes. Soil Sci. Soc. Am. J. 68, 1197–1209.

Schilling, K., Johnson, T.M., Wilcke, W., 2011. Selenium partitioning and stable isotope ratios in Urban Topsoils. Soil Sci. Soc. Am. J. 75, 1354–1364.

Schilling, K., Johnson, T.M., Wilcke, W., 2013. Isotope fractionation of selenium by biomethylation in microcosm incubations of soils. Chem. Geol. 352, 101–107.

Schilling, K., Johnson, T.M., Mason, P.R.D., 2014. A sequential extraction technique formass-balanced stable selenium isotope analysis of soil samples. Chem. Geol. 381, 125–130.

Séby, F., Potin-Gautier, M., Giffaut, E., Borge, G., Donard, O.F.X., 2001. A critical review of thermodynamic data for selenium species at 25°C. Chem. Geol. 171, 171–194.

Spark, K.M., Wells, J.D., Johnson, B.B., 1995. Characterizing trace metal adsorption on kaolinite. Eur. J. Soil Sci. 46, 633–640.

Stüeken, E.E., Foriel, J., Buick, R., Schoepfer, S.D., 2015. Selenium isotope ratios, redox changes and biological productivity across the end-Permian mass extinction. Chem. Geol. 410, 28–39.

Tan, D., Zhu, J.-M., Wang, X., Johnson, T.M., Li, S., Xu, W., 2020. Equilibrium fractionation and isotope exchange kinetics between aqueous Se(IV) and Se(VI). Geochim. Cosmochim. Acta 277, 21–36.

Tournassat, C., Ferrage, E., Poinsignon, C., Charlet, L., 2004. The titration of clay minerals II. Structure-based model and implications for clay reactivity. J. Colloid Interface Sci. 273, 234–246.

Wang, J., Han, B., Dai, M., Yan, H., Li, Z., Thomas, R.K., 1999. Effects of chain length and structure of cationic surfactants on the adsorption onto Na–Kaolinite. J. Colloid Interface Sci. 213, 596–601.

Wasylenki, L.E., Swihart, J.W., Romaniello, S.J., 2014. Cadmium isotope fractionation during adsorption to Mn oxyhydroxide at low and high ionic strength. Geochim. Cosmochim. Acta 140, 212–226.

Weerasooriya, R., Wickramarathne, H.U.S., Dharmagunawardhane, H.A., 1998. Surface complexation modeling of fluoride adsorption onto kaolinite. Colloid Surf. A 144, 267–273.

Xu, W.P., Zhu, J.-M., Johnson, T.M., Wang, X.L., Lin, Z.-Q., Tan, D.C., Qin, H.B., 2020. Selenium isotope fractionation during adsorption by Fe, Mn and Al oxides. Geochim. Cosmochim. Acta 272, 121–136.

Zhu, J.-M., Zuo, W., Liang, X., Li, S., Zheng, B., 2004. Occurrence of native selenium in Yutangba and its environmental implications. Appl. Geochem. 19, 461–467.

Zhu, J.-M., Johnson, T.M., Clark, S.K., Zhu, X.K., 2008a. High precision measurement of selenium isotopic composition by hydride generation multiple collector inductively coupled plasma mass spectrometry with a ^{74}Se-^{77}Se double Spike. Chin. J. Anal. Chem. 36, 1385–1390.

Zhu, J.-M., Wang, N., Li, S., Li, L., Su, H., Li, C., 2008b. Distribution and transport of selenium in Yutangba, China: impact of human activities. Sci. Total Environ. 392, 252–261.

Zhu, J.-M., Johnson, T.M., Finkelman, R.B., Zheng, B.-S., Sýkorová, I., Pešek, J., 2012. The occurrence and origin of selenium minerals in Se-rich stone coals, spoils and their adjacent soils in Yutangba, China. Chem. Geol. 330-331, 27–38.

Zhu, J.-M., Johnson, T.M., Clark, S.K., Zhu, X.-K., Wang, X.-L., 2014. Selenium redox cycling during weathering of Se-rich shales: a selenium isotope study. Geochim. Cosmochim. Acta 126, 228–249.

Zhu, R., Chen, Q., Zhou, Q., Xi, Y., Zhu, J., He, H., 2016. Adsorbents based on montmorillonite for contaminant removal from water: a review. Appl. Clay Sci. 123, 239–258.